*Nigerian Journal of Mathematics and Applications*
*Volume* **32** (**II**), (2022), 56 – 75. *Printed by Unilorin press*
©*Nig. J. Math. Appl.* *http* : *//www.njmaman.com*

**Special Issue in Honor of Prof. J. A. Gbadeyan's Retirement**

# Motion of Casson-Williamson with MHD Chemically Reacting Nanofluids under the Influence of Nonlinear Buoyancy Force and Theories of Cattaneo-Christov

A. S. Idowu[1*], B. O. Falodun[2], C. Onwubuoya[3] and F. O. Aiyegbusi[4]

Abstract

The focus of this research is to examine the Cattaneo-Christov heat and mass transfer processes on Casson-Williamson fluids with nonlinear buoyancy force and thermal radiation. The flow analysis was described by partial differential equations (PDEs). The resulting PDEs were simplified by utilizing suitable variables to derive coupled nonlinear total differential equations. Spectral homotopy analysis method (SHAM) was employed to solve the simplified equations. SHAM is the connections of Chebyshev differential matrix and homotopy analysis method (HAM). This research is unique because it addressed nonlinear buoyancy force significance on Casson-Williamson with Cattaneo-Christov theories with Soret-Dufour, thermal radiation, viscous dissipation, magnetic field parameter and chemical reaction. A higher Casson parameter ($\beta$) is observed to reduce the fluid velocity due to higher plastic dynamic viscosity. Increase in nonlinear buoyancy parameter for both temperature and concentration are noticed to enhance the fluid velocity.

## 1. Introduction

In view of widespread applications, a lot of interest has been shown by the researchers towards the study of non-Newtonian fluids. The main reason behind is the abundant existence of such fluids in nature as well. Non-Newtonian behavior is also used in the mining

Received: 11/06/2022, Accepted: 18/07/2022, Revised: 29/07/2022. * Corresponding author.
2015 *Mathematics Subject Classification.* 80A19 & 60G65.
*Keywords and phrases.* Casson-Williamson fluids, nonlinear buoyancy force, chemically reacting nanofluids Cattaneo-Christov and Spectral homotopy
[1]Department of Mathematics, University of Ilorin, Ilorin, Nigeria
[2&3]Department of Computer Science/Mathematics, Novena University, Ogume, Nigeria
[4]Department of Mathematics and Statistics, First Technical University, Ibadan, Nigeria
E-mails of the corresponding author: sesan@unilorin.edu.ng
ORCID of the corresponding author: 0000-0002-5634-3449

industry, where slurries and muds are often handled, and in applications such as lubrication and biomedical flows. The simulation of non-Newtonian fluid flow phenomena is therefore of importance to industry. A considerable amount of work has been done in the regime of non-Newtonian fluids and much more is needed in a variety of non-Newtonian fluid models. The rheological applications of all these fluids in chemical and engineering process has attracted many researchers in literature. [1] did a comparative study of two non-Newtonian fluids past a stretching sheet using numerical approach. They find out that the thermal conductivity has great impact on the two fluids within the boundary layer. [2] studied the flow of Casson fluid across an oscillating vertical plate with radiation and chemical reaction significance. They solved their flow equations numerically and found out that an increase in the Casson parameter leads to decrease in the fluid velocity. [3] researched on 3D Casson fluid flow past a passable linearly stretchable sheet with convective boundary constraints. [4] discussed the significance of varying viscosity and thermal conductivity on the simultaneous motion of Casson-Walters-B non-Newtonian fluids under Soret-Dufour influence. A spectral analysis approach was used and the variable viscosity and thermal conductivity was found to great affects the Casson-Walters-B when mixed together in the boundary layer. In another study of [5], the flow of MHD non-Newtonian nanofluid past an inclined plate was numerically discussed. Spectral homotopy analysis method was used to solve the governing equations. Their findings revealed that increase in thermal radiation greatly increase the temperature of the nanoparticles within the boundary layer. Numerical examination of a non-Newtonian Carreau fluid flow due to catalytic surface reactions on an upper surface with buoyancy and stretching at the free stream has been studied by [6].

Heat transfer is an everyday occurrence. It is applicable when heat flows from hot objects to cold ones and vice versa. The investigation on heat transport of liquids have attracted many researchers' in recent time. Casson non-Newtonian liquid has yield stress and viscous in nature. The blood of human being is a Casson liquid due too blood cells chain structure and protein, fibrinogen, rouleaux, etc which are the substances present in the blood. Model of heat transport of Casson liquid finds application in processing of food and drying of food. It was first proposed by [7]. [8] examined flow of Casson liquid under the influence of viscous dissipative along with convective boundary conditions and MHD. [9] studied double diffusive effects on convective mixed flow of Casson fluid. The recent study of [10] considered variable viscosity along with thermal conductivity influence on Casson nanofluid flow. [11] considered flow of Casson fluid past a vertical cone. The motion of Casson fluid with viscous dissipation effects was examined by [12]. The motion on non-Newtonian is complex because it result to nonlinearity between stress and rate of strain. Casson fluid non-Newtonian model have been considered by several authors in literature. The flow of heat, mass along with Casson non-Newtonian fluid was examined by [13]. [14] examined Casson fluid flow with suction, variable viscosity along with thermal conductivity. [15] studied MHD boundary layer flow of Casson fluid with thermal radiation. MHD is a branch of physics that examined the attitude of an electrically conducting fluid such as plasma or molten metal. It is basically acted upon on magnetic field. MHD is applicable when conductor moves into a magnetic field and electric current creates its own magnetic field. Due to the industrial along with MHD applications in areas like power generators, pumps of electromagnetic and metal coating. [16] examined MHD convective-radiative oscillatory flow. The study of [17] explained the important of MHD in free convective chemically reacting micropolar fluid flow. MHD natural convection in the generation of heat in porous medium have been investigated by [18]. [19] studied unsteady hydromagnetic chemically reacting mixed convective flow. [20] examined MHD

mixed convection flow with dissipation effect. [21] examined double-diffusive MHD flow over a stretching sheet. [22] studied MHD viscoelastic fluid flow with chemical reaction effect. [23] examined the behaviour of MHD on heat and mass transfer.
Problem on analysis of viscous dissipation in recent time have gained authors attention. The dispersion of viscosity in the boundary layer gives rise to more heat between fluid particles. Hence, the collision between fluid particles increases with higher intermolecular forces. As a result of its applications in engineering mainly in the problem of heat transfer such as heat exchangers devices, chemical catalytic reactors, petroleum reservoirs etc many researchers have investigated this phenomenon. [24] considered analysis of viscous equilibrium in heat transfer on blunted cone at hypersonic flow. [25] examined the existence of viscous dissipation in the simulation of MHD nanofluid. [26] elucidate viscous and ohmic dissipation on unsteady hydromagnetic flow. [27] examined melting along with dissipative viscous dissipation effects on MHD flow. The study of [28] extensively discussed viscous dissipation. Heat transfer involves the transfer of heat from one object to another while mass transfer phenomenon involves the transfer of fluid particles from one region to another. Heat and mass transfer (duble-diffusive) boundary layer flow has attracted many researchers because of its numerous applications in thermal and nuclear engineering. Concentration and thermal boundary layer arises when fluid temperature and concentration are distinct at the surface layer. [29] examined heat alongwith mass transfer of hydrodynamic and thermal layer flow along a flat plate. [30] researched on mixed convection of a nanofluid from an inclined wavy surface embedded in a non-Darcy passable medium. [31] researched on radiative heat transfer of variable viscosity and thermal conductivity significance on inclined magnetic field with dissipation in a non-Darcy medium. Significance of chemical rection and wall properties on MHD peristaltic transport of a dusty fluid with heat and mass transfer has been researched by [32]. [33] addressed heat and mass transfer effects on mixed concetive flow of chemically reacting nanofluid past a moving/stationaty vertical plate. [34] studied thermophoresis with double-diffusive MHD mixed convection mass transfer past an inclined plate with non-uniform heat source/sink and chemical reaction. [35] examined free convective MHD Cattaneo-Christov flow past three distinct geometries.
The significance of thermal radiation, viscous dissipation and magnetic field on the motion of Casson-Williamson nanofluids through a vertical porous plate has received little attention. Therefore, this study attempts to explore the impact of viscous dissipation, magnetic field and thermal radiation on a moving Casson-Williamson nanofluids in a vertical porous plate under the influence of thermo-physical parameters. The novelty of this research are as follows:

(1) Simultaneous flow of Casson and Williamson non-Newtonian fluids with combined influence of Soret-Dufour mechanism;
(2) Significance of nonlinear buoyancy force past a vertical porous plate; and
(3) The significance of Cattaneo-Christov theories on Casson-Williamson nanofluids motion in a vertical porous plate.

## 2. Mathematical Analysis

Consider a free convective, two-dimensional, laminar, incompressible boundary layer flow of Casson fluid through a vertical porous plate with Cattaneo-Christov heat flux (see [36] & [37]). The coordinate system of the problem are (x,y) where x-coordinate is utilized along the Riga plate while y-coordinate normal to it. The physics of the problem in a vertical stretching Riga surface is illustrated in Figure 1. $T_w$ and $C_w$ are denoted to be wall temperature and concentration while $C_\infty$ and $T_\infty$ are ambient concentration and

temperature respectively. A nonlinear buoyancy force is considered in this study with the presence of a first order chemical reaction. A screnario whereby $T_w > T_\infty$ and $C_w > C_\infty$ which means a heated Riga surface is considered in this study. The viscosity and thermal conductivity existing within the boundary layer are considered to vary. The Lorentz force is used in conjuction with Grinberg term in this study. The equations of motion for Casson-Williamson fluid are as described in this study as follows: The flow of two liquids of Casson as well as Williamson is explored. It leads to two liquids terms. Based on viscosity $\left(\tau=\mu\frac{\partial u}{\partial y}|_y=0\right)$, the rheological equation of a Casson liquid as discussed in [4] are: $\tau_{ij}=\left(\mu_b(T)+\frac{P_y}{\sqrt{2\pi}}\right)2e_{ij} \quad when \quad \pi>\pi_c$

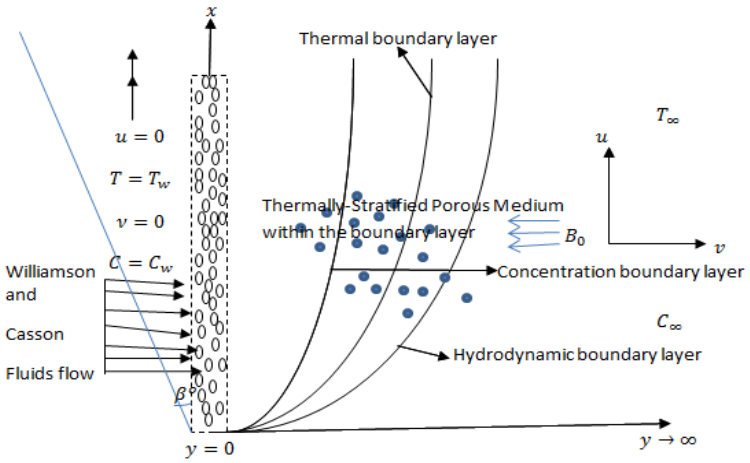


Figure 1: Physical geometry

$$\tau_{ij}=\left(\mu_b(T)+\frac{P_y}{\sqrt{2\pi_c}}\right)2e_{ij} \quad when \quad \pi<\pi_c \tag{2.1}$$

here $P_y$ signifies yield stress of the liquid which is

$$P_y=\frac{\mu_b(T)\sqrt{(2\pi)}}{\gamma} \tag{2.2}$$

$\mu_b$ indicates plastic dynamic Casson viscosity, $\pi=e_{ij}e_{ij}$ indicates the multiplication of deformation rate both together and $e_{ij}$ indicates deforming rate and $\pi_c$ indicates critical value of Casson liquid. The Casson liquid flow when $\pi>\pi_c$, we have

$$\mu_0=\mu_b(T)+\frac{P_y}{\sqrt{2\pi}} \tag{2.3}$$

invoking eqn (2.2) in (2.3), the viscosity becomes subject to plastic dynamic Casson viscosity $\mu_b$, the density $\rho$ and the Casson term $\gamma$ gives

$$\mu_0=\frac{\mu_b(T)}{\rho}\left(1+\frac{1}{\gamma}\right) \tag{2.4}$$

The fluid is set into motion because of stretching sheet. Williamson fluid constitutive equation as described by Nadeem et al. (2013) gives:

$$S=-pI+\tau \tag{2.5}$$

$$\tau = \left[\mu_\infty + \frac{(\mu_0 - \mu_\infty)}{1 - \Gamma(\dot{\gamma})}\right] A_1 \tag{2.6}$$

From which the pressure is $p$, $I$ means Identity, $\tau$ is stress tensor, $\mu_0$ is zero along with unending shear rate and $\mu_\infty$, $\Gamma>0$ signifies constant time, $A_1$ is tensor of Rivlin-Erickson and $\dot{\gamma}$ is given as

$$\dot{\gamma} = \sqrt{\frac{1}{2}\pi}, \quad where \quad \pi = trace(A_1^2) \tag{2.7}$$

$$\dot{\gamma} - \left[\left(\frac{\partial u}{\partial c}\right)^2 + \frac{1}{2}\left(\frac{\partial u}{\partial x} + \frac{\partial v}{\partial x}\right)^2 + \left(\frac{\partial v}{\partial y}\right)^2\right]^{\frac{1}{2}} = 0 \tag{2.8}$$

where $\pi=$ second invariant strain tensor. It should be noted in this study that the case when $\mu_\infty = 0$ and $\Gamma\dot{\gamma}<1$ is considered in the present study. Hence, equation (2.6) is additional stress tensor which is:

$$\tau - \left[\frac{\mu_0}{1 - \Gamma\dot{\gamma}}\right] A_1 = 0 \tag{2.9}$$

Therefore, the additional stress tensor shown in equation (2.9) as explored in [38] are:

$$\tau_{xx} - 2\mu_0[1 + \Gamma\dot{\gamma}]\frac{\partial u}{\partial x} = 0, \quad \tau xy = \tau yx = \mu_0[1 + \Gamma\dot{\gamma}]\left(\frac{\partial u}{\partial y} + \frac{\partial v}{\partial x}\right)$$

$$\tau_{yy} = 2\mu_0[1 + \Gamma\dot{\gamma}]\frac{\partial v}{\partial y}, \quad \tau xz = \tau yz = \tau zx = \tau zy = \tau zz = 0 \tag{2.10}$$

The boundary layer approximation is valid and base on the above assumptions the flow equations according to [37] becomes

$$\frac{\partial u}{\partial x} + \frac{\partial v}{\partial y} = 0 \tag{2.11}$$

(2.12)

$$\rho\left(u\frac{\partial u}{\partial x} + v\frac{\partial u}{\partial y}\right) = \mu\left(1 + \frac{1}{\gamma}\right)\frac{\partial^2 u}{\partial y^2} + \sqrt{2}\nu\Gamma\frac{\partial u}{\partial y}\frac{\partial^2 u}{\partial y^2} + g\rho\cos(\beta^o)[\beta_1(T - T_\infty) + \beta_2(T - T_\infty)^2] +$$

$$g\rho\cos(\beta^o)[\beta_3(C - C_\infty) + \beta_4(C - C_\infty)^2] - \left(\sigma B_0^2(x) + \frac{\mu}{K_p}\left(1 + \frac{1}{\beta}\right)\right)u$$

$$u\frac{\partial T}{\partial x} + v\frac{\partial T}{\partial y} = \alpha_1\frac{\partial^2 T}{\partial y^2} + \frac{Dk_T}{c_s c_p}\frac{\partial^2 C}{\partial y^2} + \frac{\mu}{\rho c_p}\left(1 + \frac{1}{\gamma}\right)\left(\frac{\partial u}{\partial y}\right)^2 - \frac{1}{\rho c_p}\frac{\partial q_r}{\partial y} + \frac{Q}{\rho c_p}(T - T_\infty) \tag{2.13}$$

$$+\tau\left[D\frac{\partial C}{\partial y}\frac{\partial T}{\partial y} + \frac{D_T}{T_\infty}\left(\frac{\partial T}{\partial y}\right)^2\right]$$

$$-h_1\left[u\frac{\partial u}{\partial x}\frac{\partial T}{\partial x} + v\frac{\partial v}{\partial y}\frac{\partial T}{\partial y} + u\frac{\partial v}{\partial x}\frac{\partial T}{\partial x} + v^2\frac{\partial^2 T}{\partial y^2} + v\frac{\partial u}{\partial y}\frac{\partial T}{\partial x} + 2uv\frac{\partial^2 T}{\partial y \partial x} + u^2\frac{\partial^2 T}{\partial y^2}\right]$$

$$u\frac{\partial C}{\partial x} + v\frac{\partial C}{\partial y} = D\frac{\partial^2 C}{\partial y^2} + \frac{Dk_T}{T_m}\frac{\partial^2 T}{\partial y^2} - K'(C - C_\infty) + \frac{D_T}{T_\infty}\frac{\partial^2 T}{\partial y^2} \tag{2.14}$$

$$-h_2\begin{bmatrix} u\frac{\partial u}{\partial x}\frac{\partial C}{\partial x}+v\frac{\partial v}{\partial y}\frac{\partial C}{\partial y}+u\frac{\partial v}{\partial x}\frac{\partial C}{\partial x} \\ +v^2\frac{\partial^2 C}{\partial y^2}+v\frac{\partial u}{\partial y}\frac{\partial C}{\partial x} \\ +2uv\frac{\partial^2 C}{\partial y\partial x}+u^2\frac{\partial^2 C}{\partial y^2} \end{bmatrix}$$

Subject to:

$$u{=}U_w(x)={B}x \quad ,v{=}-\nu(x) \quad ,T{=}T_w \quad ,C{=}C_w \quad ,at \quad y{=}0 \tag{2.15}$$

$$u\longrightarrow 0 \quad ,T\longrightarrow T_\infty \quad ,C\longrightarrow C_\infty \quad ,as \quad y\longrightarrow\infty \tag{2.16}$$

In equation (2.12) above, $\beta_1$ indicate linear convective parameter for temperature, $\beta_2$ indicates nonlinear convective term for temperature, $\beta_3$ indicates linear convective parameter for concentration, $\beta_4$ indicates nonlinear convective parameter for concentration. The temperature $(T_w)$ and concentration $(C_w)$ at the wall and free stream is defined by [37] as:

$$T_w{=}T_0+m_1x, \quad T_\infty{=}T_0+m_2x, \quad C_w{=}C_0+m_3x, \quad C_\infty{=}C_0+m_4x \tag{2.17}$$

Te relation $u$ and $v$ are defined as a function of the stream function defined as

$$u{=}\frac{\partial\psi}{\partial y}, \quad v{=}-\frac{\partial\psi}{\partial x} \quad where \quad \psi{=}\sqrt{a\nu}f(\eta)x \tag{2.18}$$

The stream function satisfies the continuity automatically. We define the variables employed here as (see [37]):

$$\eta{=}y\sqrt{\frac{a}{\nu}}, \quad \vartheta{=}\frac{T-T_0}{T_w-T_0}, \quad \varphi{=}\frac{C-C_0}{C_w-C_0} \tag{2.19}$$

Invoking equation (2.19) above into the governing flow equations (2.12)-(2.15) one obtain

$$\left(1+\frac{1}{\beta}\right)F'''{+}FF''{-}(F')^2{+}A_1\cos(\beta^{\circ})\theta^2{+}A_2\cos(\beta^{\circ})\phi^2{+}\lambda_a\cos(\beta^{\circ})\theta{+}\lambda_b\cos(\beta^{\circ})\phi \tag{2.20}$$

$$-\left(M+\frac{1}{Po}\right)f'+WeF''F'''{=}0$$

$$\left(\frac{1+R}{Pr}\right)\theta''+F\theta'+Do\phi'+Ec\left(1+\frac{1}{\boldsymbol{\beta}}\right)F''^2+\Delta\theta+Na\phi'\theta'+Nb\theta'^2 \tag{2.21}$$

$$-\alpha_1\left[FF'\theta'+FF\theta''\right]=0$$

$$\frac{1}{Sc}\phi''+f\phi'-Cr\phi+So\theta''+\frac{Nb}{LnNa}\theta''-\alpha_2\left[FF'\phi'+FF\phi''\right]=0 \tag{2.22}$$

subject to:

$$F'(\eta)=1, \quad F(\eta)={S}_w, \quad \theta(\eta)=(1-St), \quad \phi(\eta)=(1-St), \quad at \quad \eta{=}0 \tag{2.23}$$

$$F'(\eta)\longrightarrow 0, \quad \theta(\eta)\longrightarrow 0, \quad \phi(\eta)\longrightarrow 0, \quad as \quad \eta\longrightarrow\infty \tag{2.24}$$

where , $M{=}\frac{\sigma B_0^2(x)}{\rho B}$ is imposed magnetic parameter, $Po{=}\frac{K_pB}{\mu}$ is permeability parameter, $We{=}\Gamma U_w(x)\left(\frac{2B}{\nu}\right)^{\frac{1}{2}}$ is non-Newtonian Williamson parameter, $Pr{=}\frac{\nu}{\alpha}$ is Prandtl number,

$R=\frac{4\sigma_s T_\infty^2}{Ke}$ is thermal radiation parameter, $A_1=\frac{g\beta_T(T_w-T_\infty)^2}{B^2x}$ is nonlinear convective parameter for temperature, $A_2=\frac{g\beta_c(C_w-C_\infty)^2}{B^2x}$ is nonlinear convective parameter for concentration, $\lambda_a=\frac{g\beta_T(T_w-T_\infty)}{B^2x}$ is linear convective parameter for temperature, $\lambda_b=\frac{g\beta_c(C_w-C_\infty)}{B^2x}$ is linear convective parameter for concentration, $Do=\frac{Dk_T(C_w-C_\infty)}{\nu c_s c_p(T_w-T_\infty)}$ is Dufour number, $Ec=\frac{(Bx)^2}{c_p(T_w-T_\infty)}$ is Eckert number, $\Delta=\frac{Q}{\rho c_p B}$ is heat generation parameter, $Sc=\frac{\nu}{D}$ is Schmidt number, $Cr=\frac{K_l}{B}$ is chemical reaction parameter, $So=\frac{Dk_T(T_w-T_\infty)}{\nu T_m(C_w-C_\infty)}$ is Soret number, $\tau=\frac{K}{T_{ref}}$ is thermophoresis parameter, $Na=\frac{\tau D(C_w-C_\infty)}{\nu}$ is Brownian motion, $Nb=\frac{\tau D_T(C_w-C_\infty)}{T_\infty\nu}$ is the thermophoretic parameter, $Ln=\frac{\nu}{D}$ is the Lewis number.

The practical engineering interest are local skin friction coefficient $(C_f)$, Sherwood number $(Sh)$ and Nusselt number $(Nu)$. They are defined in this studies as follows:

$$C_f=\frac{\tau_w}{\rho\nu u^2} \qquad where \qquad \tau_w=\left[\left(\mu_B+\frac{P_y}{\sqrt{2\pi}}\right)+\sqrt{2}\nu\Gamma\frac{\partial^2 u}{\partial y^2}\right]\frac{\partial u}{\partial y}|_{y=0}$$

$$Nu=\frac{q_w}{\alpha_1\Delta\mathrm{T}}=\vartheta'(0) \qquad where \qquad q_w=K\left(\frac{\partial T}{\partial y}\right)_{y=0}=\alpha_1\Delta\mathrm{T}\vartheta'(0)$$

$$Sh=\frac{m_w}{\frac{D}{\nu}\Delta\mathrm{C}}=\varphi'(0) \qquad where \qquad m_w=D\left(\frac{\partial C}{\partial y}\right)_{y=0}=\frac{D}{\nu}\Delta\mathrm{C}\varphi'(0)$$

2.1. **Spectral Relaxation Technique.** The transformed coupled nonlinear ordinary differential (2.20)-(2.22) subject to (2.23) and (2.24) are solved numerically utilizing SRM. SRM is an iterative approach that uses the Gauss-seidel type's relaxation approach to decouple and linearize the coupled equations. The linearized equations will be discretized and solved by employing the Chebyshev pseudo-spectral method [38]. The degree of iteration was facilitated on all linear terms at the current iteration noted, while nonlinear terms are assumed to be known from the previous iteration noted. The basic steps of the spectral approach are:

(1) First, decouple the nonlinear equations and linearize them using Gauss-Siedel techniques;
(2) The linearized equations were further discretized, and
(3) The discretized equations are solved iteratively by utilizing the Chebyshev pseudo-spectral technique.

Applying the SRM to obtain the following:

$$a_{0,r}F'''_{r+1}+a_{1,r}F''_{r+1}-a_{2,r}+a_{3,r}+a_{4,r}-a_{5,r}F'_{r+1}+a_{6,r}F'''_{r+1}=0 \tag{2.25}$$

$$b_{0,r}\theta''_{r+1}+b_{1,r}\theta'_{r+1}+b_{2,r}+b_{3,r}+\Delta\theta_{r+1}$$

$$+b_{4,r}\theta'_{r+1}+b_{5,r}+b_{6,r}\theta'_{r+1}+b_{7,r}\theta''_{r+1}=0 \tag{2.26}$$

$$\frac{1}{Sc}\phi''_{r+1}+c_{0,r}\phi'_{r+1}-Cr\phi_{r+1}+c_{1,r}+c_{2,r}+c_{3,r}\phi'_{r+1}+c_{4,r}\phi''_{r+1}=0 \tag{2.27}$$

where the coefficient parameters are defined as follows:

$$a_{0,r}=\left(1+\frac{1}{\beta}\right), \quad a_{1,r}=F_r, \quad a_{2,r}=(F'_r)^2, \quad a_{3,r}=A_1\cos(\beta^o)\theta_r^2+A_2\cos(\beta^o)\phi_r^2$$

$$a_{4,r}=\lambda_a\cos(\beta^o)\theta_r+\lambda_b\cos(\beta^o)\phi_r,\quad a_{5,r}=\left(M+\frac{1}{Po}\right),\quad a_{6,r}=WeF''_r$$

$$b_{0,r}=\left(\frac{1+R}{Pr}\right),\quad b_{1,r}=F_{r+1},\quad b_{2,r}=Do\phi'_r,\quad b_{3,r}=Ec\left(1+\frac{1}{\beta}\right)(F''_{r+1})^2$$

$$b_{4,r}=Na\phi'_r,\quad b_{5,r}=Nb\theta'^2_r,\quad b_{6,r}=-\alpha_1F_{r+1}F'_{r+1},\quad b_{7,r}=-\alpha_1F^2_{r+1}$$

$$c_{0,r}=F_{r+1},\quad c_{1,r}=So\theta''_{r+1},\quad c_{2,r}=\frac{Nb}{LnNa}\theta''_{r+1},\quad c_{3,r}=-\alpha_2F_{r+1}F'_{r+1},\quad c_{4,r}=-\alpha_2F^2_{r+1}$$

2.2. **Outcomes and discussion.** The couple equations in (2.20)-(2.22) alongwith (2.23) and (2.24) are numerically solved by utilizing SRM. To explain clearly the physics of the problem, a parametric study was conducted and the numerical outcomes are presented graphically. Also, computations on the engineering quantities of interest are tabulated. The default values adopted in this study are: $M=1,\beta=2,We=3,R=0.4,Pr=7,Do=Sr=1.5,Ec=0.4,Sc=0.61,\alpha_1=\alpha_2=A_1=A_2=2$. Figure 2 depicts the nonlinear convective parameter for temperature $A_1$ on the velocity profile. The nonlinear upward force as exerted on the working fluid was found to oppose the weight of the fluid. As seen in Figure 2, increase in the value of the nonlinear thermall buoyancy force leads to an increased velocity profile. A higher nonlinear thermal buoyancy force a laminar flow. The upward increase in $A_1$ is observed to elevate the local skin friction in table 1 and the entire hydrodynamic boundary layer thickness. Figure 3 illustrates the nonlinear convective parameter for concentration $A_2$. In Figure 3, the nonlinear upward force was found to greatly affects the mass diffusivity of the fluid. An increase in the nonlinear mass buoyancy force greatly increases the fluid velocity to peak value. The fluid velocity profile as illustrated in figures 2 and 3 portrays a maximum value in the plate vicinity and gradually decreases as it approaches the free stream.

This research work examined the Cattaneo-Christov theories on double-diffusive flow. The thermal relaxation time ($\alpha_1$) as illustrated in Figure 4 shows that increase in $\alpha_1$ enhances both velocity and temperature distributions. Practically, the two non-Newtonian fluids considered in this study moves into the boundary layer simultaneously with a constant temperature. As a result of collision, the temperature of fluid particles increases alongside the momentum gathered within the boundary layer. The thermal relaxation time added more heat energy to the boundary layer, hence the hydrodynamic and thermal boundary layer increases. Figure 5 illustrates the mass relaxation time ($\alpha_2$) on the velocity and concentration distributions. The mass diffusivity of the fluid was greatly affected by $\alpha_2$ and hereby enhances the species boundary layer. A distinctive maximum value is obstained on the graphical result for velocity and concentration due to increase in $\alpha_2$. Figure 6 illustrates the impact of Soret parameter ($Sr$) on the velocity and concentration distributions. From Figure 6, the velocity distribution increases within the boundary layer due to increase in $Sr$. Remarkably, a rise in fluid velocity is noticeable as a result of greater thermal diffusion. Furthermore, the concentration profile rises due to an increase in Soret number. Figure 7 depicts the significance of Dufour number ($Do$) on the velocity and temperature distributions. It is observed in Figure 7 that the diffusion thermal effect causes increase to fluid velocity and temperature respectively. Th significance of Sr and Do are observed to be opposite in heat and mass transfer phenomenon.

Figure 8 shows the significance of Eckert number ($Ec$) on the velocity and temperature distributions. The Eckert number ($Ec$) is the relationship existing on the flow enthalpy

and kinetic energy. This enables the kinetic energy to be converted into internal energy energy due to work done. An increase in Ec leads to greater viscous dissipative heat, from which it is concluded that increase in $Ec$ leads to a rise in the fluid velocity and temperature. Figure 9 illustrates the significance of thermal radiation on the velocity and temperature distributions. The presence of $R$ in this study enhances convective flow. Thermal radiation is of great significance at a very high temperature. A high intensity of $R$ is observed to raise the fluid temperature and the entire thermal boundary layer thickness. However, the increase in R leads to an enhancement in the fluid thermal condition which leads to a rise in fluid velocity and the hydrodynamic boundary layer thickness. Figure 10 illustrates the significance of Prandtl number ($Pr$) on the velocity and temperature distributions. Physically, $Pr$ explains the connection between the thermal conductivity and kinematic viscosity. A greater thermal conductivity and kinematic viscosity propeled $Pr$ to reduce the temperature of fluids. In Figure 10, increase in Pr declines the hydrodynamic and thermal boundary layer thickness. The significance of Schmidt number ($Sc$) on the velocity and concentration distributions are illustrated in Figure 11. Mathematically, $Sc = \frac{\nu}{D}$ where $\nu > D$ indicates higher $Sc$ and vice versa. Physically, the rate of mass transfer declines as a result of concentration buoyancy significance. Due to this fact, the concentration distribution decreases.

Figure 12 portrays the significance of magnetic field parameter (M) on the velocity distribution. The imposed magnetic field plays a significant role on the flow of an electrically conducting fluids (Casson-Williamson) by giving rise to Lorentz force. The Lorentz force hereby slows down the motion of Casson-Williamson fluids. The physics of magnetic impact as depicted in Figure 12 portrays decrease in fluid velocity. Figure 13 illustrates the impact of Casson parameter ($\boldsymbol{\beta}$) on the velocity distribution. In the present analysis, the imposed magnetic plays a significant role on the Casson fluid by causing reduction to the fluid velocity. The plastic dynamic viscosity also cause a reverse flow on the fluid. Therefore, increase in $\boldsymbol{\beta}$ declines the velocity profile. Figure 14 shows the impact of Williamson parameter ($We$). A higher value of We is observed to enhance the velocity and the entire bydrodynamic boundary layer thickness.

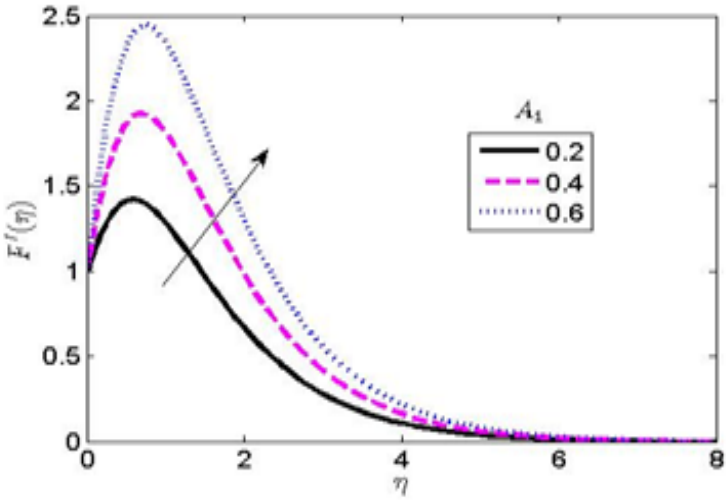


Figure 2: Significance of nonlinear convective parameter for temperature on velocity profile

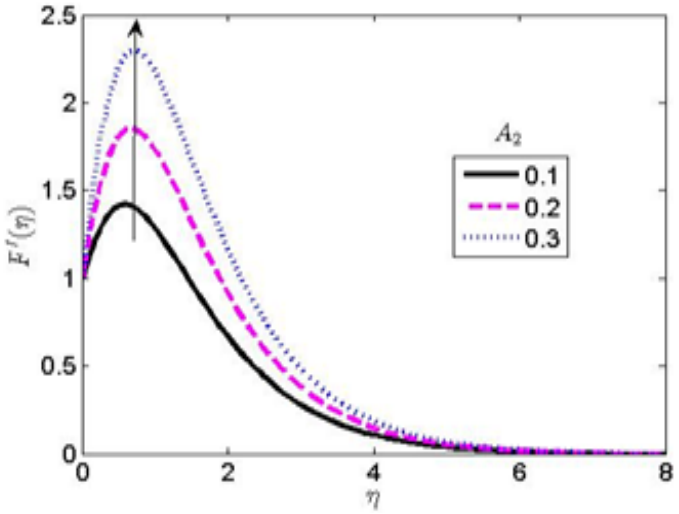


Figure 3: Significance of nonlinear convective parameter for concentration on velocity profile

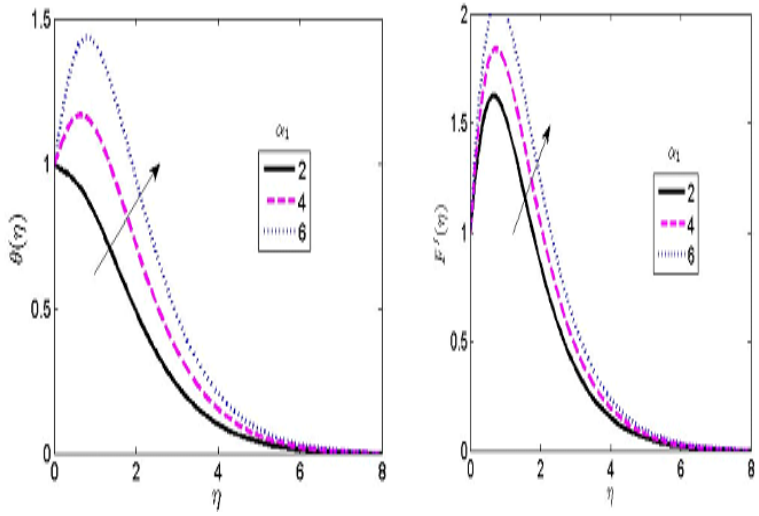


Figure 4: Significance of thermal relaxation time on the temperature and velocity profiles

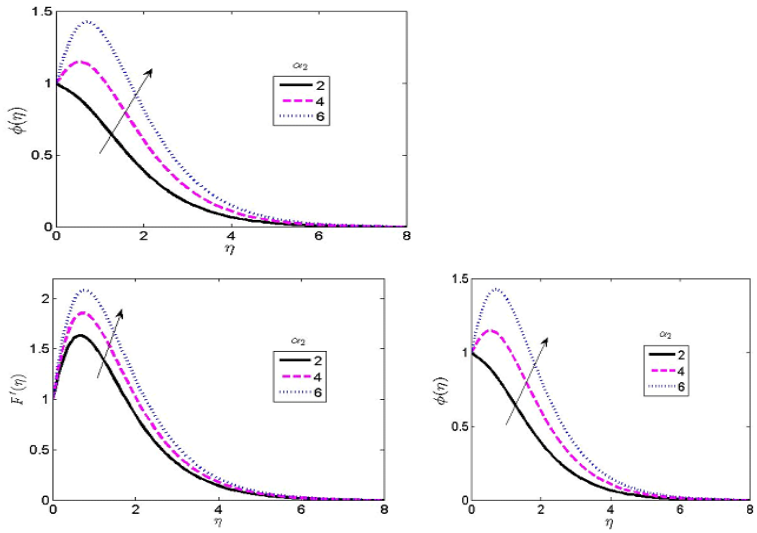


Figure 5: Significance of mass relaxation time on the concentration and velocity profiles

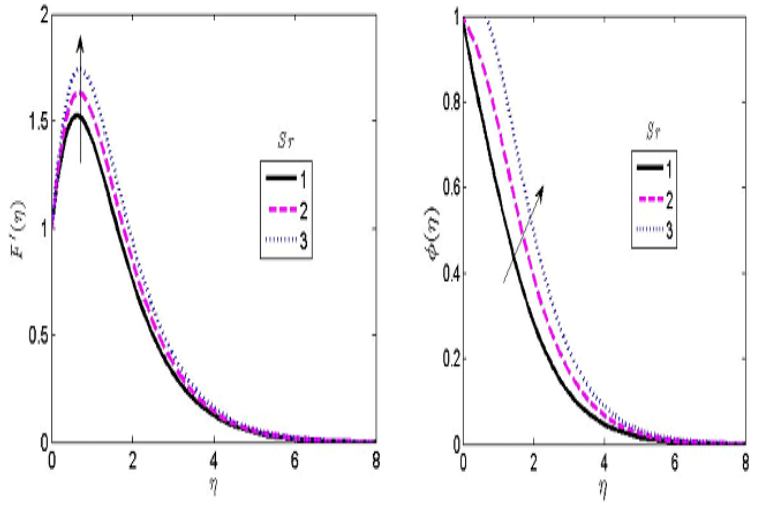


Figure 6: Significance of Soret parameter on the velocity and concentration profiles

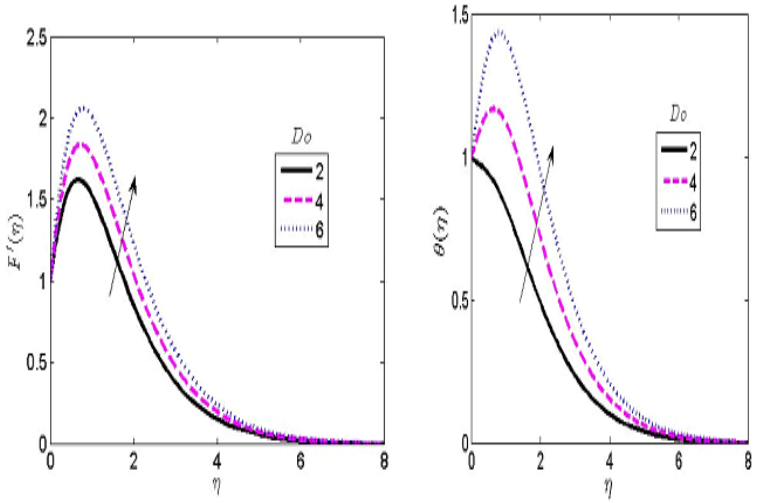


Figure 7: Significance of Dufour parameter on the velocity and temperature profiles

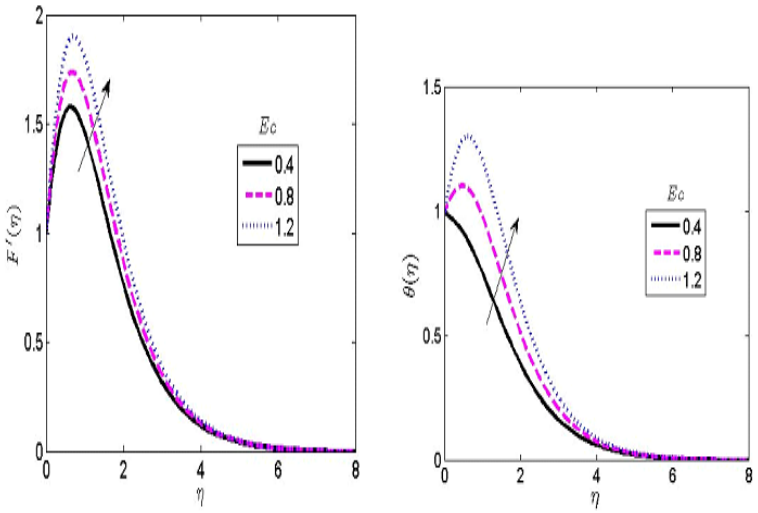


Figure 8: Significance of Eckert number on the velocity and temperature profiles

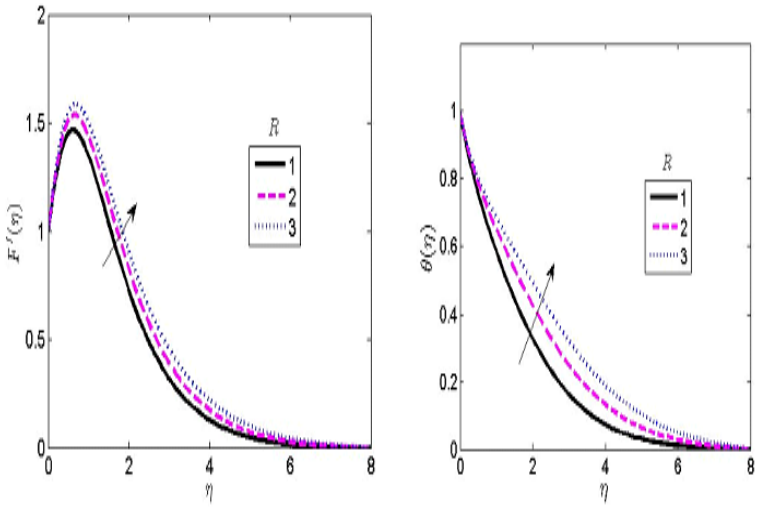


Figure 9: Significance of thermal radiation on the velocity and temperature profiles

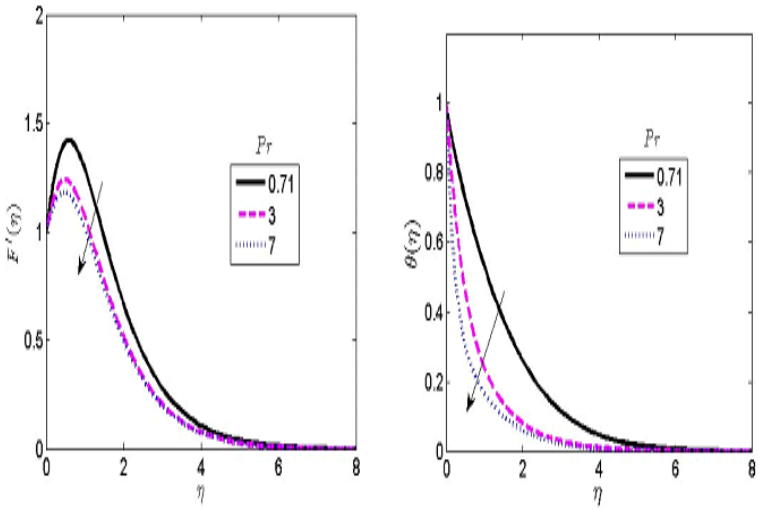


Figure 10: Significance of Prandtl number on the velocity and temperature profiles

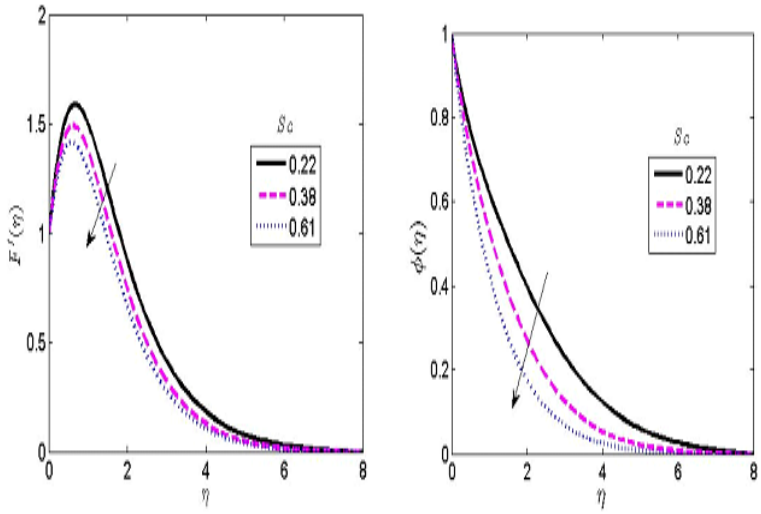


Figure 11: Significance of Schmidt number on the velocity and concentration profiles

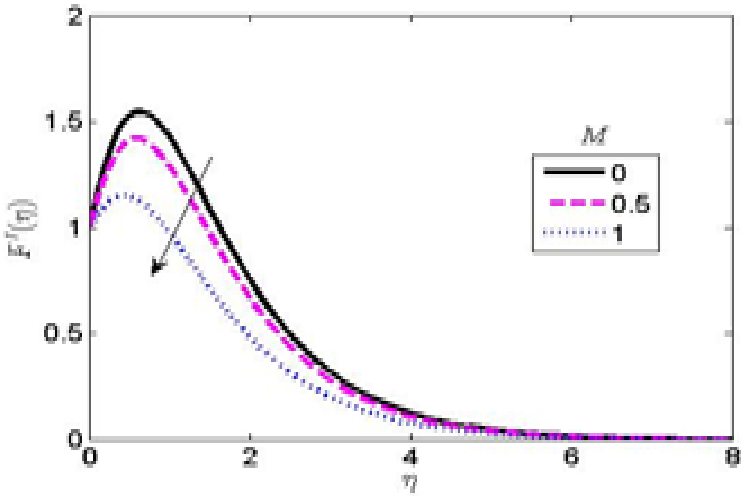


Figure 12: Significance of Magnetic field on the velocity profile

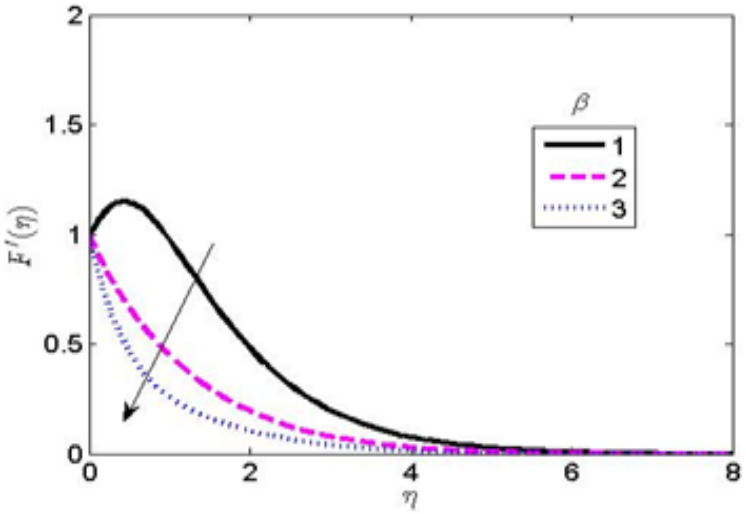


Figure 13: Significance of Casson parameter on the velocity profile

**Table 1:** Computational values for local skin friction (Cf), local Nusselt number (Nu) and local Sherwood number for variations of pertinent flow parameters.

| M | $\boldsymbol{\beta}$ | We | R | Pr | Do | Sr | Ec | Sc | $\boldsymbol{\alpha_1}$ | $\boldsymbol{A_1}$ | $\boldsymbol{A_2}$ | $\boldsymbol{\alpha_2}$ | Cf | Nu | Sh |
|---|---|---|---|---|---|---|---|---|---|---|---|---|---|---|---|
| 0.0 | | | | | | | | | | | | | 1.7682 | 0.4921 | 0.3417 |
| 0.5 | | | | | | | | | | | | | 1.4328 | 0.4921 | 0.3417 |
| 1.0 | | | | | | | | | | | | | 0.6530 | 0.4921 | 0.3417 |
| | 1.0 | | | | | | | | | | | | 0.8242 | 0.5123 | 0.6981 |
| | 2.0 | | | | | | | | | | | | 1.7939 | 0.5123 | 0.6981 |
| | 3.0 | | | | | | | | | | | | 1.8345 | 0.5123 | 0.6981 |
| | | 1.0 | | | | | | | | | | | 1.6906 | 0.5745 | 0.8121 |
| | | 2.0 | | | | | | | | | | | 1.8747 | 0.5473 | 0.8121 |
| | | 3.0 | | | | | | | | | | | 1.9888 | 0.5488 | 0.8121 |
| | | | 0.5 | | | | | | | | | | 1.5399 | 0.5543 | 0.8633 |
| | | | 1.0 | | | | | | | | | | 1.6900 | 0.5745 | 0.8633 |
| | | | 1.5 | | | | | | | | | | 1.7955 | 0.6299 | 0.8633 |
| | | | | 0.71 | | | | | | | | | 1.4328 | 0.6935 | 0.7966 |
| | | | | 3.0 | | | | | | | | | 0.9461 | 1.5919 | 0.7966 |
| | | | | 7.0 | | | | | | | | | 0.7373 | 3.1771 | 0.7966 |
| | | | | | 1.0 | | | | | | | | 1.9145 | 0.1430 | 0.8133 |
| | | | | | 2.0 | | | | | | | | 2.3962 | 0.4075 | 0.8133 |
| | | | | | 3.0 | | | | | | | | 2.8779 | 0.9580 | 0.8133 |
| | | | | | | 1.0 | | | | | | | 1.9443 | 0.6935 | 0.2074 |
| | | | | | | 2.0 | | | | | | | 2.4558 | 0.6935 | 0.4484 |
| | | | | | | 3.0 | | | | | | | 2.9673 | 0.6935 | 1.1043 |
| | | | | | | | 0.3 | | | | | | 1.8285 | 0.1793 | 0.8033 |
| | | | | | | | 0.6 | | | | | | 2.2243 | 0.3350 | 0.8033 |
| | | | | | | | 1.0 | | | | | | 2.6202 | 0.8494 | 0.8033 |
| | | | | | | | | 0.6 | | | | | 1.8171 | 0.9918 | 0.6223 |
| | | | | | | | | 1.0 | | | | | 1.6072 | 0.9918 | 0.7169 |
| | | | | | | | | 2.0 | | | | | 1.4265 | 0.9918 | 0.8701 |
| | | | | | | | | | 0.2 | | | | 0.9141 | 0.2400 | 0.7010 |
| | | | | | | | | | 0.3 | | | | 1.3960 | 0.4012 | 0.7010 |
| | | | | | | | | | 0.4 | | | | 2.8111 | 0.5011 | 0.7010 |
| | | | | | | | | | | 0.0 | | | 1.4328 | 0.9918 | 0.7968 |
| | | | | | | | | | | 0.5 | | | 2.7985 | 0.9918 | 0.7968 |
| | | | | | | | | | | 1.0 | | | 4.1643 | 0.9918 | 0.7968 |
| | | | | | | | | | | | 0.0 | | 2.4021 | 0.8299 | 0.5197 |
| | | | | | | | | | | | 0.5 | | 2.6370 | 0.8299 | 0.5197 |
| | | | | | | | | | | | 1.0 | | 3.8412 | 0.8299 | 0.5197 |
| | | | | | | | | | | | | 1.0 | 2.9221 | 0.6101 | 1.2074 |
| | | | | | | | | | | | | 2.0 | 3.5501 | 0.6101 | 2.4480 |
| | | | | | | | | | | | | 3.0 | 4.9611 | 0.6101 | 3.1043 |

**Table 2**: Comparison of the present results with Spectral relaxation method (SRM) and that of [37] with Spectral homotopy analysis method (SHAM) when $\beta = A_1 = A_2 = Po = We = R = Do = \Delta = Na = Nb = \alpha_1 = So = Ln = \alpha_2 = 0$.

| Gr | M | Present study (SRM) | | | [37] (SHAM) | | |
|---|---|---|---|---|---|---|---|
| | | $-f'(0)$ | $-\theta'(0)$ | $-\phi'(0)$ | $-f'(0)$ | $-\theta'(0)$ | $-\phi'(0)$ |
| 0.0 | 0.0 | 1.21162127 | 0.59172593 | 2.80851599 | 1.21162126 | 0.59172594 | 2.80851598 |
| | 0.5 | 1.38842065 | 0.58861360 | 2.81200614 | 1.38842063 | 0.58861361 | 2.81200613 |
| | 1.0 | 1.49482308 | 0.58611500 | 2.81550166 | 1.49482305 | 0.58611501 | 2.81550165 |
| | 2.0 | 1.74371572 | 0.58195569 | 2.82145445 | 1.74371569 | 0.58195570 | 2.82145444 |
| 0.5 | 0.0 | 0.99357637 | 0.60035148 | 2.80004023 | 0.99357636 | 0.60035150 | 2.80004022 |
| | 0.5 | 1.15480104 | 0.59645010 | 2.80502274 | 1.15480103 | 0.59645010 | 2.80502273 |
| | 1.0 | 1.30255127 | 0.59327759 | 2.80931154 | 1.30255126 | 0.59327761 | 2.80931153 |
| | 2.0 | 1.56865628 | 0.58830966 | 2.81645989 | 1.56865626 | 0.58830968 | 2.81645988 |
| 1.0 | 0.0 | 0.77921445 | 0.60843711 | 2.79183852 | 0.77921446 | 0.60843714 | 2.79183851 |
| | 0.5 | 0.95371215 | 0.60357740 | 2.79758673 | 0.95371217 | 0.60357743 | 2.79758672 |
| | 1.0 | 1.11214612 | 0.59968276 | 2.80247588 | 1.11214615 | 0.59968279 | 2.80247587 |
| | 2.0 | 1.39474829 | 0.59368080 | 2.81052221 | 1.39474832 | 0.59368083 | 2.81052220 |
| 2.0 | 0.0 | 0.30028109 | 0.62317674 | 2.77616511 | 0.30028108 | 0.62317678 | 2.77616510 |
| | 0.5 | 0.55844229 | 0.61682733 | 2.78323090 | 0.55844228 | 0.61682737 | 2.78323091 |
| | 1.0 | 0.73651538 | 0.61174060 | 2.78919280 | 0.73651536 | 0.61174064 | 2.78919279 |
| | 2.0 | 1.05019015 | 0.60394790 | 2.79889283 | 1.05019013 | 0.60394794 | 2.79889282 |

**Conclusions:** Analysis of Cattaneo-Christov theories on Casson-Williamson fluids with nonlinear buoyancy force with different flow parameters are examined using PDEs and solved by utilizing SHAM. The simultaneous flow of Casson-Williamson fluids as illustrated in Figure 1 enters through the vertical porous plate into the boundary layer. The viscosity and thermal conductivity are considered to be constant within th boundary layer. The choice of SHAM is due to its efficiency and flexibility in chosing linear operators as compare with other methods in literature. Key findings in this study are:

(1) Increase in $\boldsymbol{\beta}$ slows down the velocity distribution because of higher plastic dynamic viscosity which opposes the fluid motion;
(2) It is observed that, the imposed magnetic field declines the motion of fluids within the boundary layer;
(3) A higher Sc is observed to decrease the rate of mass transfer;
(4) Increase in the thermal relaxation time is observed to enhance the hydrodynamic and the specie boundary layer thickness;
(5) The Eckert number is observed to give rise to heat energy which enhances the fluid temperature; and
(6) The nonlinear buoyancy force for temperature and concentration is noticed to bring increase to the fluid velocity.

.

**Acknowledgement:** We acknowledged all authors we made reference to their works and thank all the authors of this work for their painstakingly contributed to the work. And thank our mentor Prof Gbadeyan for the opportunity to train under him.

**Competing interests:** The content of the manuscript was approved by all authors. Therefore, no competing interest between authors.

**Funding:** The Authors received no financial support for the research, authorship, and/or publication of this article.

## Nomenclature

| | |
|---|---|
| $u$ | velocity in x-axis (Unit: $m/s$) |
| $v$ | velocity in y-axis (Unit: $m/s$) |
| $g$ | gravity |
| $K$ | permeability term |
| $D_m$ | mass diffusivity (Unit: $m^2s^{-1}$ |
| $B_0$ | magnetic constant |
| $c_p$ | specific heat (Unit: $J/kgk$) |
| $q_r$ | heat flux (Unit: $W/m^2$) |
| $k_T$ | thermal diffusion ratio |
| $c_s$ | Solutal susceptibility (Unit: $kmolm^{-3}$) |
| $K'$ | chemical coefficient (Unit:$kmolm^{-3}$) |
| $T_m$ | mean fluid temperature (Unit:$K$) |
| $B$ | Constant |
| $Q$ | heat generation term |
| $S_w$ | suction velocity (Unit: $m/s$) |
| $\beta_1, \beta_3$ | Linear convective parameter for temperature and concentration |
| $\beta_2, \beta_4$ | Nonlinear convective parameter for temperature and concentration |
| $T$ | temperature (Unit: K) |
| $C$ | concentration (Unit: $m^2s^{-1}$) |
| $T_\infty$ | ambient temperature (Unit: $K$) |
| $C_\infty$ | ambient concentration (Unit:$mol$) |
| $\sigma$ | electrical conductivity |
| $\rho$ | density (Unit: $kg/m^3$) |
| $\nu$ | viscosity (Unit: $m^2/s$) |
| $\psi$ | stream function (Unit: $m^2/s$) |
| $\eta$ | similarity variable (Unit: dimensionless) |
| $T_w$ | temperature at the wall(Unit: K) |
| $C_w$ | Concentration at the wall (Unit: $mole$) |
| $\vartheta(\eta)$ | Temperature in dimensionless form |
| $\varphi(\eta)$ | Concentration in dimensionless form |
| $\mu_0$ | coefficient of viscosity (Unit: $m^2/s$) |
| $\gamma$ | Casson parameter |

## References


[1] Reddy Ramana J. V., Anantha Kumar K., Sugunamma V. & Sandeep N. (2018). Effect of cross diffusion on MHD non-Newtonian fluids flow past a stretching sheet with non-uniform heat source/sink: A comparative study. *Alexandria Engineering Journal*. **57**, 1829-1838.

[2] Hari R. Kataria & Harshad R. Patel (2016). Radiation and chemical reaction effects on MHD Casson fluid flow past an oscillating vertical plate embedded in porous medium. *Alexandria Engineering Journal*. **55**, 583-595.

[3] Mahanta G. & Shaw S. (2015). 3D Casson fluid flow past a porous linearly stretching sheet with convective boundary condition. *Alexandria Engineering Journal*. **54**, 653-659.

[4] Idowu, A. S. & Falodun, B. O. (2020a). Variable thermal conductivity and viscosity effects on non-Newtonian fluids flow through a vertical porous plate under Soret-Dufour influence. *Mathematics and Computers in Simulation*. **177**, 358-384.

[5] Idowu A. S. & Falodun B. O. (2020b). Effects of thermophoresis, Soret-Dufour on heat and mass transfer flow of magnetohydrodynamics non-Newtonian nanofluid over an inclined plate. *Arab Journal of Basic and Applied Sciences*. **27** (1), 149-165, DOI: 10.1080/25765299.2020.1746017.

[6] Animasaun I. L. & Pop I. (2017). Numerical exploration of a non-Newtonian Carreau fluid flow driven by catalytic surface reactions on an upper horizontal surface of a paraboloid of revolution, buoyancy and stretching at the free stream. *Alexandria Engineering Journal*. **56**, 647-658.

[7] Casson N. (1959). *A Flow Equation for Pigment-Oil Suspensions of the Printing Ink Type, In: Mill, C.C., Ed., Rheology of Disperse Systems*. Pergamon Press, Oxford, 84-104.

[8] Neeraja A., Renuka Devi R. L. V., Devika B., Naga Radhika V. & Krishna Murthy, M. (2019). Effects of viscous dissipation and convective boundary conditions on magnetohydrodynamics flow of casson liquid over a deformable porous channel. *Results in Engineering*. **4**, 100040.

[9] Prasad D. V. K., Krishna Chaitanya G. S. & Srinivasa Raju R. (2019). Double diffusive effects on mixed convection Casson fluid flow past a wavy inclined plate in presence of Darcian porous medium, . *Results in Engineering*. **3**, 100019.

[10] Gbadeyan J. A., Titiloye E. O. & Adeosun, A.T. (2020). Effect of variable thermal conductivity and viscosity on Casson nanofluid flow with convective heating and velocity slip. *Heliyon*. **6**, e03076.

[11] Mythili D., Sivaraj R., Rashidi M. M. & Yang Z. (2015). Casson fluid flow over a vertical cone with non-uniform heat source/sink and high order chemical reaction. *Journal of Naval Architecture and Marine Engineering*. **15**, 125-136, http://dx.doi.org/10.3329/jname.v12i2.25269.

[12] Ajayi T. M., Omowaye A. J. & Animasaun I. L. (2017). Viscous Dissipation Effects on the Motion of Casson Fluid over an Upper Horizontal Thermally Stratified Melting Surface of a Paraboloid of Revolution:Boundary Layer Analysis. *Journal of Applied Mathematics*. **2017**, Article ID 1697135, 13 pages https://doi.org/10.1155/2017/1697135.

[13] Raju C. S. K., Sandeep N., Sugunamma V., Jayachandra Babu M. & Ramana Reddy J. V. (2015). Heat and mass transfer in magnetohydrodynamic Casson fluid over an exponentially permeable stretching surface. *Engineering Science and Technology, an International Journal* (Article in Press).

[14] Animasaun I. L. (2015). Effects of thermophoresis, variable viscosity and thermal conductivity on free convective heat and mass transfer of non-darcian MHD dissipative Casson fluid flow with suction and nth order of chemical reaction. *Journal of the Nigerian Mathematical Society*. **34** 11-31.

[15] Mukhopadhyay S., Iswar Chandra Moindal & Tasawar Hayat (2014). MHD boundary layer flow of Casson fluid passing through an exponentially stretching permeable surface with thermal radiation. *Chin. Phys. B*. **23** (10), 104701.

[16] Pal Dulal & Sukanta Biswas (2018). Magnetohydrodynamic convective-radiative oscillatory flow of a chemically reactive micropolar fluid in a porous medium. *Propulsion and Power Research*. **7** (2), 158-170.

[17] Sheri S. R., Shamshuddin M. D. (2018). Finite element analysis on transient magnetohydrodynamic(MHD)free convective chemically reacting micropolar fluid flow pasta vertical porous plate with Hall current and viscous dissipation. *Propulsion and Power Research*. **7** (4), 353-365.

[18] Ahmed S. E. & Rashed Z. Z. (2019). MHD natural convection in a heat generating porous medium-filled wavy enclosures using Buongiorno's nanofluid model. *Case Studies in Thermal Engineering*. **14**, 100430.

[19] Daba M. & Ponnaian Devaraj (2016). Unsteady hydromagnetic chemically reacting mixed convection flow over a permeable stretching surface with slip and thermal radiation. *Journal of the Nigerian Mathematical Society*. **35**, 245-256.

[20] Bhukta D., Dash G. C., Mishra S. R. & Baag S. (2017). Dissipation effect on MHD mixed convection flow over a stretching sheet through porous medium with non-uniform heat source/sink. *Ain Shams Engineering Journal*. **8**, 353-361.

[21] Sreedevi G., Raghavendra Rao R., Prasada Rao D. R. V. & Chamkha, A. J. (2016). Combined influence of radiation absorption and Hall current effects on MHD double-diffusive free convective flow past a stretching sheet. *Ain Shams Engineering Journal*. **7**, 383-397.

[22] Jena S., Dash G. C. & Mishra S. R. (2018). Chemical reaction effect on MHD viscoelastic fluid flow over a vertical stretching sheet with heat source/sink. *Ain Shams Engineering Journal*. **9**, 1205-1213.

[23] Idowu A. S. & Falodun B. O. (2018). Soret-Dufour effects on MHD heat and mass transfer of Walter's-B viscoelastic fluid over a semi-infinite vertical plate: spectral relaxation analysis. *Journal of Taibah University for Science*, DOI: 10.1080/16583655.2018.1523527.

[24] Pish F., Hassanvand A., Barzegar Gerdroodbary M. & Noori S. (2019). Viscous equilibrium analysis of heat transfer on blunted cone at hypersonic flow. *Case Studies in Thermal Engineering*. **14**, 100464.

[25] Alsagri A. S., Hassanpour A. & Abdulrahman A. Alrobaian (2019). Simulation of MHD nanofluid flow in existence of viscous dissipation by means of ADM. *Case Studies in Thermal Engineering*. **14**, 100494.

[26] Devi Anjali S. P. & Vasantha Kumari D. (2018). Thermal radiation, viscous dissipation, ohmic dissipation and mass transfer effects on unsteady hydromagnetic flow over a stretching surface. *Ain Shams Engineering Journal*. **9**, 1161-1168.

[27] Venkateswarlu B., Satya P. V. & Narayana Nainaru Tarakaramu (2018). Melting and viscous dissipation effects on MHD flow over a moving surface with constant heat source. *Transactions of A. Razmadze Mathematical Institute*. **172**, 619-630.

[28] Alao F. I., Fagbade A. I. & Falodun B. O. (2016). Effects of thermal radiation, Soret and Dufour on an unsteady heat and mass transfer flow of a chemically reacting fluid past a semi-infinite vertical plate with viscous dissipation. *Journal of the Nigerian Mathematical Society*. **35**, 142-158.

[29] Oyelami Funmilayo H. & Falodun Bidemi O. (2021). Heat and Mass Transfer of Hydrodynamic boundary layer flow along a flat plate with the influence of variable temperature and viscous dissipation. *International Journal of Heat and Technology*. **39** (2), 441-450.

[30] Srinivasacharya D. & Vijay Kumar P. (2018). Effect of thermal radiation on mixed convection of a nanofluid from an inclined wavy surface embedded in a non-Darcy porous medium with wall heat flux. *Propulsion and Power Research*. **7** (2), 147-157.

[31] Muthuraj R., Nirmala K. & Srinivas S. (2016). Influences of chemical reaction and wall properties on MHD Peristaltic transport of a Dusty fluid with Heat and Mass transfer. *Alexandria Engineering Journal*. **55**, 597-611.

[32] Mahanthesh B., Gireesha B. J., Rama Subba & Reddy Gorla Gorla (2016). Heat and mass transfer effects on the mixed convective flow of chemically reacting nanofluid past a moving/stationary vertical plate. *Alexandria Engineering Journal*. **55**, 569-581.

[33] Mondal Hiranmoy, Dulal Pal, Sewli Chatterjee & Precious Sibanda (2018). Thermophoresis and Soret-Dufour on MHD mixed convection mass transfer over an inclined plate with non-uniform heat source/sink and chemical reaction. *Ain Shams Engineering Journal*. **9**, 2111-2121.

[34] Jayachandra Babu M., Sandeep N. & Saleem, S. (2017). Free convective MHD Cattaneo-Christov flow over three different geometries with thermophoresis and Brownian motion. *Alexandria Engineering Journal*. **56**, 659-669.

[35] Gladys Tharapatla, Pamula Rajkumari, Gurrampati V. Ramanareddy (2021). Effects of heat and mass transfer on MHD nonlinear free convection non-Newtonian fluids flow embedded in a thermally stratified porous medium. *Heat Transfer*. 1-21.

[36] Falodun B. O. & Omowaye A. J. (2019). Double-diffusive MHD convective flow of heat and mass transfer over a stretching sheet embedded in a thermally-stratified porous medium. *World Journal of Engineering*. **16** (6), 712-724.

[37] Nadeem S, Rizwan Ul Haq, Noreen Sher Akbar, Khan Zh (2013). MHD three-dimensional Casson fluid flow past a porous linearly stretching sheet. *Alexandria Engineering Journal*. **52**, 577-582.

[38] Motsa S. S. (2012). *New iterative methods for solving nonlinear boundary value problems. Fifth annual workshop on computational applied mathematics and mathematical modelling in fluid flow*. School of Mathematics, Statistics and Computer Science, Pietermaritzburg Campus.